ELSEVIER

Inorganica Chimica Acta 288 (1999) 159–173

Inorganica Chimica Acta

Isocyanide derivatives of manganese cobalt nonacarbonyl: synthesis and characterization

Karsten Beck [1], John J. Alexander *, Jeanette A. Krause Bauer, Jeffrey L. Nauss [2]

Department of Chemistry, University of Cincinnati, Cincinnati, OH 45221, USA

Received 12 June 1998; accepted 1 February 1999

Abstract

The synthesis and spectral characterization of isocyanide derivatives of $MnCo(CO)_9$ of the type $MnCo(CO)_{9-n}(CNR)_n$ ($n = 1,2$; R = (*p*-$MeOC_6H_4$)NC, (2,6-xylyl)NC, (t-butyl)NC, (n-butyl)NC, (2,6-diisopropylphenyl)NC) are reported. The X-ray structure of $MnCo(CO)_8$((2,6-xylyl)NC) (**1**) and $MnCo(CO)_7$((2,6-xylyl)NC)$_2$ (**2**) are reported herein as well. The structures of **1** and **2** contain a single metal–metal bond and no bridging ligands. The length of the Mn–Co bond is 2.870(1) and 2.9035(7) Å in **1** and **2**, respectively. The IR spectra of $Mn(CO)_5Br$, $Mn_2(CO)_{10}$, $MnCo(CO)_9$ and $MnCo(CO)_{9-n}(CNR)_n$ ($n = 1,2$; R = CH_3) were calculated using density functional theory. The calculated IR spectra were employed to assign the structure of the $MnCo(CO)_{9-n}$-$(CNR)_n$ ($n = 1,2$) compounds. © 1999 Elsevier Science S.A. All rights reserved.

Keywords: Crystal structures; Manganese complexes; Cobalt complexes; Carbonyl complexes; Isocyanide complexes

1. Introduction

Transition metal carbonyl complexes are of interest as homogeneous catalysts [1]. Multimetallic complexes should theoretically have advantages over mononuclear complexes. For example, they have the ability to form multicenter metal-to-ligand bonds to a substrate, thus assisting in the activation of that species toward further reactions. Multimetallic complexes also offer the possibility for the selective and sequential activation of two (or more) different substrate species [2].

Isocyanides, CNR, are isolobal with CO and often are able to displace CO in transition metal complexes. Isocyanides contain an organic group R, which can be altered to fine tune the metal complex electronically and sterically. Isocyanides are considered to be stronger σ-donors, and weaker π-acceptors than CO [3].

The reactions of $Mn_2(CO)_{10}$ [4], $Re_2(CO)_{10}$ [5] and $Co_2(CO)_8$ [6] with CNR have previously been investigated. In the case of $M_2(CO)_{10}$ (M = Mn, Re) complexes of the type $M_2(CO)_{10-n}(CNR)_n$ ($n = 1$–4) (R = alkyl, aryl) were obtained. In no case could more than four carbonyls be substituted by isocyanides. By contrast, reaction of $Co_2(CO)_8$ with CNR gave the disproportionation product $[Co(CNR)_5]^+[Co(CO)_4]^-$ at room temperature and the completely substituted product $Co_2(CNR)_8$ (R = 2,6-xylyl) at 80°C.

The structures of the Mn and Re compounds show a single metal–metal bond, no bridging ligands, and staggered arrangement of the eight equatorial ligands [4,5]. The isocyanide ligands are always equatorial and, if on the same metal, *cis* to each other. The structures of $Co_2(CNR)_8$ (R = 2,6-xylyl, t-butyl) resemble that of $Co_2(CO)_8$, with six terminal isocyanides and two bridging isocyanides [6,7].

Since the chemistry of $Co_2(CO)_8$ towards CNR is so different compared to that of $M_2(CO)_{10}$ (M = Mn, Re), it seemed interesting to investigate the reactions of CNR with $MnCo(CO)_9$ [8]. Especially, we were interested in whether substitution occurs preferentially on the manganese site or on the cobalt site. Another point of interest was whether CNR-substituted Mn–Co carbonyl complexes would contain any bridging ligands, similar to the structure of $Co_2(CNR)_8$, or only terminal

* Corresponding author. Tel.: +1-513-556 9200; fax: +1-513-556 9239.

[1] Present address. Department of Chemistry, University of Michigan, Ann Arbor, MI 48103-1055.

[2] Present address. Molecular Simulations, Inc., 9685 Scranton Road, San Diego, CA 92121-3752.

PII: S0020-1693(99)00081-X

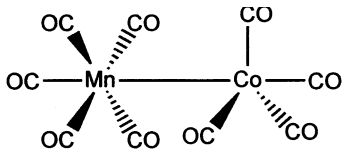

Fig. 1. Structure of $MnCo(CO)_9$.

ligands similar to $M_2(CO)_{10}$ and $M_2(CO)_{10-n}(CNR)_n$ ($n = 1$–4) (M = Mn, Re).

$MnCo(CO)_9$ is believed to have C_s symmetry (Fig. 1), although no X-ray data have been reported for $MnCo(CO)_9$ or any unbridged derivative. The proposed structure is based on the compound's IR spectrum, and the ^{55}Mn and ^{59}Co NMR. The local site symmetry is C_{3v} at the cobalt site, and C_{4v} at the manganese site [9].

In contrast to $Co_2(CO)_8$ and $M_2(CO)_{10}$ (M = Mn, Re), the metal–metal bond in $MnCo(CO)_9$ is polarized, with a partial negative charge on cobalt [9]. This increases the electron density around Co in $MnCo(CO)_9$ compared to $Co_2(CO)_8$. Consistent with this interpretation is the fact that the carbonyl stretching force constants on the $Co(CO)_4$ moiety in $MnCo(CO)_9$ are calculated to be lower than the values found in $Co_2(CO)_8$ (non-bridged isomer), $HCo(CO)_4$, and $CH_3Co(CO)_4$, indicating increased back donation [10,11].

This publication reports the synthesis and characterization of isocyanide-substituted derivatives of $MnCo(CO)_9$. The calculated IR spectra of $MnCo(CO)_9$ and of its CNR substituted derivatives using density functional theory (DFT) methods are presented herein as well. Furthermore, the crystal structures of $MnCo(CO)_8$((2,6-xylyl)NC) (**1**) and $MnCo(CO)_7$((2,6-xylyl)NC)$_2$ (**2**) are reported.

2. Experimental

2.1. General experimental details, materials, and analysis of the products

All reactions were done under an argon atmosphere. Tetrahydrofuran (THF), toluene and hexane were distilled from potassium benzophenone ketyl. Benzene and CH_2Cl_2 were distilled from P_2O_5. Diethyl ether was anhydrous grade (Fisher) and used as received. All other solvents were reagent grade and used as received. $Mn_2(CO)_{10}$ and $Co_2(CO)_8$ were purchased from Strem. Me_3NO was purchased from Eastman, benzene-d_6 from Acros, acetone-d_6 from Cambridge Isotope Laboratories and $CDCl_3$ from Aldrich. (2,6-xylyl)NC was purchased from Fluka. (t-butyl)NC [12], (p-$MeOC_6H_4$)NC [12], (2,6-diisopropylphenyl)NC [12], (n-butyl)NC [13], $NaCo(CO)_4$ [14], $NaCo[(2,6\text{-xylyl})NC]_4$ [15], $Mn(CO)_5Br$ [16] and $Mn(CO)_{5-n}(CNR)_nBr$ ($n = 1$–4) [17] were synthesized by published methods. $MnCo(CO)_9$ was prepared according to a literature method [18], except that diethyl ether was used instead of THF as the solvent. Silica gel 60, 230–400 mesh, from EM science and Aluminum Oxide 90, active basic grade 1, (alumina) were used for column chromatography.

Infrared spectra were recorded on a Perkin–Elmer 1600 Series FTIR spectrophotometer. IR cells were 1.0 mm solution cells with NaCl windows. For spectral intensities the abbreviations vw = very weak, s = strong, vs = very strong are used. ^1H NMR data were recorded using a Bruker AM-250 spectrometer. The following abbreviations are used: m = multiplet, s = singlet.

The complexes $MnCo(CO)_{9-n}(CNR)_n$ ($n = 1, 2$) are temperature sensitive. They slowly decompose at room temperature and must be stored in the freezer at −25°C. Therefore satisfactory elemental analysis could not be obtained for all complexes. Still, since the IR and ^1H NMR data of all $MnCo(CO)_8(CNR)$ complexes are consistent with **1**, and the IR and ^1H NMR data of all $MnCo(CO)_7(CNR)_2$ complexes are consistent with **2**, we feel confident that the synthesized complexes were correctly identified as $MnCo(CO)_{9-n}(CNR)_n$ ($n = 1, 2$). Elemental analyses were performed by Quantitative Analysis, Whitehouse, NJ, and the results are presented in Table 1.

2.2. Synthesis of $MnCo(CO)_{9-n}(CNR)_n$ ($n = 1, 2$)

2.2.1. Procedure A (R = (p-$MeOC_6H_4$)NC, (2,6-xylyl)NC, (t-butyl)NC, (n-butyl)NC)

$MnCo(CO)_9$ (0.15 mmol, 54.9 mg) was dissolved in benzene (10 ml) in the presence of PdO (5% mol). The appropriate number of equivalents of CNR, dissolved

Table 1
Elemental analysis

	Calc. (found) C	Calc. (found) H	Calc. (found) N
$MnCo(CO)_7$((2,6-xylyl)NC)$_2$ (**2**)	52.47 (51.57)	3.15 (3.12)	4.89 (4.57)
$MnCo(CO)_8$(p-$MeOC_6H_4$)NC (**9**)	40.80 (40.10)	1.50 (1.62)	2.97 (2.89)
$MnCo(CO)_8$((2,6-diisopropylphenyl)NC) (**8**)	48.02 (46.99)	3.26 (3.44)	2.67 (2.74)
$[Mn((2,6\text{-xylyl})NC)_6]^+[Co(CO)_4]^-$ (**5**)	68.77 (67.78)	5.37 (5.00)	8.30 (8.01)

in 3 ml of benzene, was then added dropwise. The reaction mixture was stirred at room temperature and monitored by IR. The reaction was terminated when all of the $MnCo(CO)_9$ was consumed. The solvent was removed in vacuo. Column chromatography (alumina, eluent pentane) gave the desired products. The yields of the crude products were ~25%. Multiple recrystallizations from pentane at −70°C yielded highly pure $MnCo(CO)_{9-n}(CNR)_n$ as orange solids, or dark red oils ($n=1$; R = (t-butyl)NC (**3**), (n-butyl)NC) (**4**)).

2.2.2. Procedure B (R = (t-butyl)NC, (2,6-xylyl)NC, (p-MeOC$_6$H$_4$)NC, (2,6-diisopropylphenyl)NC)

To a suspension of $Mn(CO)_{5-n}(CNR)_nBr$ (1.00 mmol) in diethyl ether, freshly prepared $NaCo(CO)_4$ (~1.5 mmol) in diethyl ether was added via cannula. The reaction mixture was stirred overnight at room temperature. The solvent was removed in vacuo and the residue was chromatographed on alumina. Elution with pentane gave the products in ~30% yield. Multiple recrystallizations from pentane at −70°C yielded highly pure $MnCo(CO)_{9-n}(CNR)_n$ as orange solids, or dark red oils (**3** and **4**).

2.3. Synthesis of $MnCo(CO)_{9-n}$((2,6-xylyl)NC)$_n$ (n = 1,2)

The reaction was run according to procedure B. Instead of alumina, silica gel was used for column chromatography. Elution with hexane/THF (5%) gave two fractions in order of elution. 55.0 mg of **1** (6%) and 43.0 mg of **2** (4%) were isolated as orange solids.

*2.4. Synthesis of $[Mn((2,6\text{-xylyl})NC)_6]^+[Co(CO)_4]^-$ (**5**)*

To a solution of $MnCo(CO)_9$ (50.0 mg; 0.137 mmol) in benzene (10.0 ml), in the presence of PdO (5% mol), 11 equivalents of (2,6-xylyl)NC were added. The reaction mixture was stirred at reflux temperature for two hours. The white precipitate was filtered off and washed with pentane. Recrystallization from CH_2Cl_2/pentane yielded 81 mg (59%) of **5** as a white solid.

IR (CH_2Cl_2): ν(CN) 2080 cm^{-1} (vs); ν(CO) 1889 cm^{-1} (s). [17]: [Mn(2,6-xylyl-NC)][PF_6]: IR (CH_2Cl_2): 2075 cm^{-1} (vs); 1996 cm^{-1} (vw) ^{1}H NMR ($CDCl_3$): 7.1 (m) C_6H_3 (3H), 2.44(s) Me (6H).

2.5. Computational details

Calculations were carried out by employing the DMol program through the INSIGHT II 95 (Version 4.0.0) graphical interface, both by Molecular Simulations [19a]. Geometries were optimized before vibrational frequencies were calculated. Atomic orbitals were described by DNP basis sets, comparable in quality to Gaussian 6-31G** basis sets [19b]. The calculations were carried out at different levels of theory: the local density approximation by Vosko–Wilk–Nusair (VWN) [20], the gradient-corrected exchange functional by Becke (B) [21], gradient-corrected correlation functionals of Perdew and Wang (PW) [22] and Lee et al. (LYP) [23]. The COSMO model by Klamt et al. was used to account for solvation effects [24]. The following combinations of functionals were used: VWN, BPW, BYLP, BVWN, VWN-COSMO (CCl_4, cyclohexane, diethyl ether, $CHCl_3$) for $Mn(CO)_5Br$; VWN and VWN-COSMO (CCl_4) for $Mn_2(CO)_{10}$, and VWN-COSMO (CCl_4) for all other compounds. Harmonic vibrational frequencies are computed by diagonalizing the mass-weighted second-derivative matrix **F**. All intensities are reported in units of km mol^{-1}.

2.6. X-ray diffraction study

For X-ray examination and data collection, a suitable crystal was mounted in a glass capillary. The approximate dimensions were $0.21 \times 0.20 \times 0.18$ mm (**1**) and $0.45 \times 0.20 \times 0.25$ mm (**2**).

Crystallographic data for **1** and **2** are presented in Table 2.

Intensity data were collected at room temperature on a Siemens SMART [25][3] CCD diffractometer (platform goniostat with χ fixed at 54.70°, sealed-tube generator, graphite-monochromated Mo Kα radiation, $\lambda = 0.71073$ Å). The detector was set at a calibrated distance of 4.959 cm from the crystal. A series of 20-s data frames measured at 0.3° increments of ω were collected with three different 2θ and ϕ values to calculate a preliminary unit cell.

For data collection 2082 data frames were measured at 0.3° intervals of ω for a 20-s duration each. In order to correct for high-energy backgrounds in the images, data frames were collected as the sum of two 10-s exposures and non-correlating events were eliminated. The data frames were collected in four distinct shells ($2\theta = -30.0°$, $\omega = -30.0°$, $\phi = 0.0$, 90.0, 180.0, 270.0°, $\chi = 54.70°$), which combined measured nearly one sphere (completeness: 93.56% (**1**); 91.4% (**2**)) of intensity data (reflections: 10 523 (**1**); 13 696 (**2**)) with a maximum θ value of 28.29°. The initial 100 frames of the first data shell were recollected at the end of the data collection to correct for crystal decay (negligible amount in the case of both samples).

[3] The SMART and SAINT programs were used for data collection and processing, respectively.

The data frames were processed using the program SAINT [25]. The data were corrected for decay, Lorentz and polarization effects. A semi-empirical absorption correction was applied using SADABS [26] (correction: min. transmission 0.7357, max. transmission 0.9489 (**1**); min. transmission 0.5718, max. transmission 0.9280 (**2**)).

The structures were solved and tables and figures generated by a combination of direct methods using SHELXTL v5.03 [27] and the difference Fourier technique and refined by full-matrix least-squares on F^2 for the unique reflections (4661 (**1**); 6360 (**2**)) diffracting to 0.75 Å resolution. Non-hydrogen atoms were refined with anisotropic displacement parameters. The phenyl moieties exhibit large thermal motion associated with a number of carbon atoms; however, possible disorder was not addressed. Weights were assigned as $w^{-1} = \sigma^2(F_o^2) + (aP)^2 + bP$ where $P = 0.33333F_o^2 + 0.66667F_c^2$ and $a = 0.0450$, $b = 0.0000$ (**1**) or $a = 0.0428$, $b = 0.6186$ (**2**). For **1** an extinction correction of the form $kF_c[1 + 0.0001\chi F_c^2\lambda^3/\sin(2\theta)]^{-1/4}$ where $k = 0.28435$, $\chi = 0.0021(11)$ was applied. Also for **1**, hydrogen atom positions were located directly from the difference map. One methyl group exhibits disordered hydrogen positions and occupancies were fixed at 0.5. In the case of **2**, hydrogen atom positions were calculated based on a geometric criterion for the electron density map. All methyl hydrogen groups have disordered hydrogen positions and occupancies were fixed at 0.5.

All hydrogen atoms were allowed to ride on their respective atoms. Hydrogen atom isotropic temperature factors were refined as $U(C)a = U(H)$ where $a = 1.5$ for methyl hydrogens and $a = 1.2$ for the remaining hydrogens. The refinement converged with crystallographic agreement factors of $R_1 = 5.63\%$, $wR_2 = 9.98\%$ and $S = 1.112$ for 2373 reflections for **1**, and $R_1 = 5.23\%$, $wR_2 = 10.71\%$ and $S = 1.065$ for 4013 reflections for **2**, with $I \geq 2\sigma(I)$ and 325 variable parameters. A final difference Fourier map showed maximum residual electron density of 0.304 e Å^{-3} (**1**) and 0.522 e Å^{-3} (**2**).

Table 2
Crystallographic data and structure refinement for **1** and **2**

Empirical formula	$C_{17}H_9CoMnNO_8$ (**1**)	$C_{25}H_{18}CoMnN_2O_7$ (**2**)
Formula weight	469.12	572.28
Temperature (K)	297(2)	273(2)
Wavelength (Å)	0.71073	0.71073
Crystal system	triclinic	triclinic
Space group	$P\bar{1}$	$P\bar{1}$
Unit cell dimensions		
a (Å)	9.786(1)	8.618(1)
α (°)	72.11(1)	90.55(1)
b (Å)	10.669(1)	9.374(1)
β (°)	85.18(1)	100.51(1)
c (Å)	10.743(1)	17.425(1)
γ (°)	64.95(1)	106.56(1)
Volume	965.6(2)	1323.8(2)
Z (Å^3)	2	2
Density (calc.) (Mg m^{-3})	1.613	1.436
Absorption coefficient (mm^{-1})	1.556	1.148
$F(000)$	486	580
Crystal size (mm)	$0.21 \times 0.20 \times 0.18$	$0.45 \times 0.25 \times 0.20$
θ Range for data collection (°)	2.21–28.29	2.50–28.29
Limiting indices	$-13 \leq h \leq 12$	$-11 \leq h \leq 11$
	$-14 \leq k \leq 14$	$-12 \leq k \leq 12$
	$-14 \leq l \leq 14$	$-23 \leq l \leq 23$
Reflections collected	10523	13696
Independent reflections	4661 ($R_{int} = 0.0546$)	6360 ($R_{int} = 0.0310$)
Refinement method	full-matrix least-squares on F^2	full-matrix least-squares on F^2
Data/restraints/parameters	4661/0/254	6360/0/325
Goodness-of-fit on F^2	1.006	1.065
Final R indices [$I > 2\sigma(I)$]		
R_1	0.0563	0.0523
wR_2	0.0998	0.1071
R indices (all data)		
R_1	0.1382	0.0960
wR_2	0.1269	0.1280
Largest difference peak, hole (e Å^{-3})	0.304, −0.320	0.522, −0.284
Extinction coefficient	0.0021(11)	

3. Results and discussion

3.1. Synthesis of $MnCo(CO)_{9-n}(CNR)_n$ (n = 1,2)

3.1.1. The compounds $MnCo(CO)_8(CNR)$ and $MnCo(CO)_7(CNR)_2$

(R = *p*-$MeOC_6H_4$; 2,6-xylyl; t-butyl; n-butyl) were obtained from the reaction of $MnCo(CO)_9$ and CNR in benzene (Eq. (1)), in the presence of PdO. PdO is known to catalyze CO substitutions by CNR [4]. The complexes are orange solids, except for $MnCo(CO)_8(CNR)$ (R = t-butyl (**3**), n-butyl (**4**)), which melt at $\sim 15-20$°C.

$$MnCo(CO)_9 + nCNR \rightarrow (MnCo(CO)_{9-n}(CNR)_n + nCO \quad (n = 1,2) \quad (1)$$

Other solvents did not give satisfactory results. In CH_2Cl_2, toluene and acetonitrile metal–metal bond cleavage occurred, indicated by the presence of a strong, broad band at $\sim 1900\ cm^{-1}$ in the IR spectrum due to $Co(CO)_4^-$. Apparently these solvents promote the nucleophilic substitution of $Co(CO)_4^-$ by CNR. In hexane, the reaction yielded an unidentified mixture of compounds. In diethyl ether, using (*p*-$MeOC_6H_4$)NC, only a very small amount of $MnCo(CO)_7$((*p*-$MeOC_6H_4$)NC)$_2$ (**6**) could be isolated. It is somewhat surprising that, out of the solvents tested, only benzene gives a clean reaction; however, Coville et al. made similar observations when they allowed $Mn_2(CO)_{10}$ to react with CNR in the presence of PdO [4a].

Me_3NO is also known to promote the substitution of CO by CNR in metal carbonyl complexes [28]. Nonetheless, all attempts to synthesize $MnCo(CO)_{9-n}(CNR)_n$ employing Me_3NO failed. For R = (2,6-xylyl)NC only **5** could be isolated, even after heating up the reaction mixture to 50°C for 1 hour. In the case of R = t-butyl an unidentified mixture of compounds, containing $Co(CO)_4^-$ (broad band at $\sim 1900\ cm^{-1}$), could be detected by IR. Attempts to separate this mixture were unsuccessful. Apparently, terminal COs in $MnCo(CO)_9$ are not sufficiently electrophilic to be attacked by Me_3NO.

Attempts to synthesize complexes of the type $MnCo(CO)_{9-n}(CNR)_n$ with $n > 2$ were equally unsuccessful. The reaction of 3 or 4 equivalents of (2,6-xylyl)NC with $MnCo(CO)_9$ gave only the disubstituted product **2**. However, when 3 equivalents (n-butyl)NC were used, cleavage of the metal–metal bond occurred even when the reaction was run in benzene in the presence of PdO. We suggest that $[Mn(CO)_3((n\text{-butyl})NC)_3]^+[Co(CO)_4]^-$ is the main product of the reaction. This conclusion is based on the fact that three bands in the ν(CN) (2222, 2188 and 2165 cm^{-1}), three bands in the ν(CO) region (2033, 1973 and 1966 cm^{-1}), and a strong, broad band at 1890 cm^{-1}, due to $Co(CO)_4^-$, are visible in the IR spectrum of the reaction mixture. Attempts to purify the product were unsuccessful. A ^1H NMR spectrum could not be obtained, due to paramagnetic impurities which led to line broadening. In an attempt to achieve CO substitution on the Mn site of $[Mn(CO)_3((n\text{-butyl})NC)_3]^+[Co(CO)_4]^-$ by $[Co(CO)_4]^-$, the reaction mixture was irradiated with UV light for 2.5 h. Only decomposition of the carbonyl complex could be detected by IR.

All carbonyls in $Co_2(CO)_8$ can be substituted by CNR [6]. In an attempt to achieve complete substitution in $MnCo(CO)_9$, 11 equivalents of (t-butyl)NC or (2,6-xylyl)NC were allowed to react with $MnCo(CO)_9$ in benzene/PdO under reflux conditions. (2,6-xylyl)NC yielded **5** as a white powder in high yield, whereas (t-butyl)NC gave only unidentified decomposition products.

To determine the substitution site of the CNR in the complexes $MnCo(CO)_{9-n}(CNR)_n$, the following reaction (Eq. (2)) was performed in diethyl ether:

$$Mn(CO)_{5-n}(CNR)_nBr + NaCo(CO)_4 \rightarrow (MnCo(CO)_{9-n}(CNR)_n + NaBr \quad (2)$$

($n = 1$–3) (R = t-butyl; 2,6-xylyl; *p*-$MeOC_6H_4$; 2,6-diisopropylphenyl)

For $n = 1,2$ the IR spectra of $MnCo(CO)_{9-n}(CNR)_n$ were the same, independent of the synthetic pathway (A or B). This shows that the substitution of CO by CNR takes place at the Mn center. It is interesting to note that substitution of CO in $MnCo(CO)_9$ by PPh_3 takes place at the Co center. Furthermore, the following reaction (Eq. (3)) did not yield the (PPh_3)-substituted MnCo carbonyl complex [18].

$$Mn(CO)_4(PPh_3)Br + NaCo(CO)_4 \xrightarrow{X} (MnCo(CO)_8(PPh_3) + NaBr \quad (3)$$

Still, van Dijik et al. reported the successful synthesis of $(CO)_4CoMn(CO)_3$(2,2′-bipyridine) via the reaction of $Mn(CO)_3$(2,2′-bipyridine)Br with $NaCo(CO)_4$ [29].

In the reaction mixture of Eq. (2) only traces of $Mn_2(CO)_{10}$, and no sign of the formation of $Co_2(CO)_8$ could be detected. This indicates that the reaction proceeds via nucleophilic substitution of Br^- by $Co(CO)_4^-$ and not through radical intermediates.

When one equivalent of $Mn(CO)_2(CNR)_3Br$ (R = (t-butyl), (2,6-xylyl)) was allowed to react with 1.5 equivalents of $NaCo(CO)_4$, only $MnCo(CO)_7(CNR)_2$ could be isolated. Coville et al. obtained similar results for the reaction of $M_2(CO)_{10}$ (M = Mn,Re) with CNR [4,5].

Reaction 2 gives better yields in general than Reaction 1. Reaction 2 was run in THF and in diethyl ether. The yields in diethyl ether were better than in THF,

and the reaction time was much shorter. The precipitation of NaBr, formed during the reaction, is presumably the main driving force. NaBr is seemingly less soluble in diethyl ether than in THF, since THF is a more polar solvent than diethyl ether. Therefore NaBr presumably precipitates more rapidly and more completely in diethyl ether than in THF, speeding up the reaction and increasing the yield.

The reaction of $NaCo(CO)_4$ and $Mn(CO)_4$((2,6-xylyl)NC)Br not only yielded **1**; surprisingly, disubstituted **2** was also isolated. The latter complex must have been formed during workup, because its CO stretching bands did not appear in the IR spectrum of the reaction mixture. After testing different materials for column chromatography, silica gel was selected for the workup of this reaction. Apparently reaction occurred on the column, since it got very hot. The color of the band eluted with pentane changed from dark red to brown–red upon elution. Very low yields of the mono- and disubstituted complexes were isolated.

In an attempt to synthesize Mn–Co carbonyl complexes CNR substituted at the Co site $[Co((2,6\text{-xylyl})NC)_4]^-$ was prepared from $Co_2((2,6\text{-xylyl})NC)_8$ using the methods of Cooper and coworkers [15]. $[Co((2,6\text{-xylyl})NC)_4]^-$ was then allowed to react with $Mn(CO)_5Br$; the expected product was $MnCo(CO)_5((2,6\text{-xylyl})NC)_4$. The IR spectrum of the reaction mixture exhibited 13 mostly medium to weak bands in the carbonyl region, indicating a mixture of compounds. Attempts to separate the mixture proved to be unsuccessful, and no product could be isolated.

3.2. ^1H NMR spectra

The ^1H NMR spectra of the $MnCo(CO)_{9-n}(CNR)_n$ complexes agree with the proposed structures. The chemical shifts of the coordinated isocyanide ligands are listed in Table 3 and are only slightly different from those of the uncooordinated ligands. However, the ^1H NMR signals of $CH_3–CH_2–CH_2–CH_2–NC$ in complex **4** are significantly shifted upfield ($\delta = \sim 1.7$ ppm). The ^1H NMR spectra of **3** and $MnCo(CO)_7$((t-butyl)NC)$_2$ (**7**) exhibit a singlet for the methyl protons, unlike the free isocyanide, which exhibits a 1:1:1 triplet due to nitrogen(^{14}N)-hydrogen coupling ($\delta = 1.40$; $J =$ 2.1 Hz; acetone-d_6) [30]. The fact that only one signal for all methyl protons of (2,6-xylyl)NC and (t-butyl)NC is seen in the spectrum, indicates that all protons are equivalent; hence the isocyanide ligands rotate freely around the $R_3C–NCMn$ bond.

3.3. IR spectra and computational studies

Group theory is commonly employed to predict the number of IR-active bands of molecules. For mononuclear transition metal carbonyl complexes the predictions agree well with the experiment. For bimetallic complexes the number of IR bands predicted by group theory and the number of bands observed experimentally are often different. This is either due to the fact that the bimetallic complexes deviate from the ideal symmetry assumed in the predictions or due to overlap of bands.

Density functional theory (DFT) has been used extensively to calculate vibrational frequencies of mononuclear transition metal carbonyl complexes, because it is computationally less expensive than ab initio methods [31]. For example, Fan and Ziegler calculated the vibrational spectra of $Ni(CO)_4$ and $Cr(CO)_6$ [31a]. The CO stretching frequencies were calculated by local density approximation (LDA) method and nonlocal (NL) methods, including correction terms based on electron density gradients. All calculated CO stretching frequencies were lower than the observed frequencies by 12–53 cm^{-1}. The CO stretching frequencies for $Fe(CO)_3(\eta^4$-butadiene) and $Fe(CO)_3(\eta^4$-norbornadiene) calculated by Thiel and Bühl employing NL methods deviated between 12 and 4 cm^{-1} from the experimental values [31b]. Some of the calculated values were lower and some were higher than the experimental values, with no general pattern of deviation. Bercés calculated the vibrational spectrum of $W(CO)_6$ by LDA and NL methods [31c]. The calculated CO stretching frequencies deviated between 2 and 83 cm^{-1} from the experimental values and were, except for one value, too low. Jonas and Thiel reported the calculated vibrational spectra for several transition-metal hexacarbonyls, employing NL methods [31d]. For $Mn(CO)_6^+$ and $Re(CO)_6^+$ the calculated CO stretching frequencies were too low by between 2 and 24 cm^{-1}, compared to the experimental values. In all cases, the numbers of bands were well reproduced. For the calculations of $Ni(CO)_4$, $Cr(CO)_6$, $Mn(CO)_6^+$ and $Re(CO)_6^+$ the relative IR intensities tally with the experimental values [31a,d]. The relative IR intensities for $W(CO)_6$, $Fe(CO)_3(\eta^4$-butadiene), and $Fe(CO)_3(\eta^4$-norbornadiene) were not reported [31b,c].

As a check on the structures of the parent and substituted MnCo dimers, we used DMol software module to calculate their IR spectra and compare with experimental values. A convenient feature of the DMol program is the graphical interface with Insight II, whereby the calculated normal modes of vibration can be visualized as arrow-style pictures. $Mn(CO)_5Br$ was utilized to calibrate the program parameters, since this molecule has been extensively studied by IR and since the calculation of its IR spectrum was computationally less expensive than for any binuclear complex. The results are given in Table 4.

The frequencies calculated by gradient-corrected DFT methods were significantly lower (~ 75 cm^{-1}) than the experimental values. However, the relative intensities were reasonable. The calculations involving

Table 3
^{1}H NMR data

Compound	^{1}H NMR[a]	Solvent
$MnCo(CO)_8$(2,6-(xylyl)NC) (**1**)	7.12–7.22 (m) (C_6H_3) 2.45 (s) (Me)	$CDCl_3$
$MnCo(CO)_8$(t-(butyl)NC) (**3**)	1.53 (s) (Me)	$CDCl_3$
$MnCo(CO)_8$(n-(butyl)NC) (**4**)	−0.71 (m) (CH_2) −0.19 (m) (CH_2) −0.07 (m) (CH_2) 3.64 (m) (Me)	acetone-d_6
$MnCo(CO)_8$(2,6-(diisopropyl)phenylNC) (**8**)	6.74–6.92 (m) (C_6H_3) 3.23 (septet) (CH) 1.09 (s) (Me) 1.07 (s) (Me)	benzene-d_6
$MnCo(CO)_8$(*p*-$MeOC_6H_4NC$) (**9**)	6.64 (ABq, $J = 12$ Hz) (C_6H_4) 6.22 (ABq, $J = 12$ Hz) (C_6H_4) 3.00 (s) (Me)	benzene-d_6
$MnCo(CO)_8$(*p*-MeC_6H_4NC) (**11**)	6.63 (m) (C_6H_4) 6.48 (m) (C_6H_4) 1.78 (s) (Me)	benzene-d_6
$MnCo(CO)_7$(2,6-(xylyl)NC)$_2$ (**2**)	7.10–7.22 (m) (C_6H_3) 2.47 (s) (Me)	$CDCl_3$
$MnCo(CO)_7$(*p*-$MeOC_6H_4NC$)$_2$ (**6**)	7.36 (ABq, $J = 12$ Hz) (C_6H_4) 6.90(ABq, $J = 12$ Hz) (C_6H_4) 3.84 (s) (Me)	$CDCl_3$
$MnCo(CO)_8$(t-(butyl)NC)$_2$ (**7**)	1.53 (s) (Me)	$CDCl_3$
$MnCo(CO)_7$(n-(butyl)NC)$_2$ (**12**)	0.98 (m) (CH_2) 1.56 (m) (CH_2) 1.80 (m) (CH_2) 3.90 (m) (Me)	acetone-d_6
$MnCo(CO)_7$(2,6-(diisopropyl)phenylNC)$_2$ (**13**)	6.82–6.89 (m) (C_6H_3) 3.48 (septet) (CH) 1.15 (s) (Me) 1.14 (s) (Me)	benzene-d_6
$[Mn(2,6\text{-(xylyl)NC})_6]^+[Co(CO)_4]^-$ (**5**)	7.16 (s) (C_6H_3) 2.43 (s) (Me)	CD_3CN

[a] Shifts reported in ppm downfield relative to TMS internal standard ($CDCl_3$, CD_3CN), or relative to the solvent peak of residual H (benzene-d_6, acetone-d_6). Abbreviations: m, multiplet; s, singlet, q, quartet.

VWN and COSMO gave the most satisfactory results. However, the calculated frequencies for the A_1 bands were higher than observed while the E band was lower, both in CCl_4 and in $CHCl_3$ solvents. To check the parameters for a binuclear complex, the IR spectrum of $Mn_2(CO)_{10}$ was calculated using VWN and COSMO. The data are presented in Table 5, and the frequencies show good agreement with the experimental values, although they are all slightly too high (~ 30 cm^{-1}). The experimental CO stretching frequencies for $Mn_2(CO)_{10}$ are on an average of 11 cm^{-1} higher in the gas phase than in CCl_4 solution. The DMol calculations show a similar trend, as the CO stretching frequencies in the VWN calculations are on an average of 9 cm^{-1} higher than in the VWN-COSMO (CCl_4) calculations. The discrepancies between calculated and observed spectra are comparable to those in the other studies reported in the literature.

The IR spectrum of $MnCo(CO)_9$ exhibits six bands in the ν(CO) region instead of the nine bands predicted by group theory for C_s symmetry. The symmetry assignments of the individual ν(CO) for the experimental values in Table 6 are taken from Ref. [18]. Employing a so called 'free rotational model' [33] allows the bands at 2025.8 and 1981.0 cm^{-1} to be labeled E modes. The basic principle of this model is the accidental degeneracy of all equatorial ν(CO) force constants on each separate metal, the vanishing of certain off-diagonal elements of the **F** matrix and the fortuitous equality of others. This approach reduces the number of predicted ν(CO) to seven (4A + B + 2E), of which six (4A + 2E) are IR active.

The IR spectrum was calculated for the C_s symmetry predicted by Moosberry and Sheline [9] (Fig. 1), and for a hypothetical C_{4v} symmetry (Fig. 2).

We wanted to test whether the experimental results agreed better with calculated results for the 'correct' structure (C_s) than for the 'wrong' structure (C_{4v}) and

Table 4
IR data for $Mn(CO)_5Br$[a,b]

Band symmetry in C_{4v}[c]	Experimental (CCl_4/$CHCl_3$)[d]	Calc. VWN	Calc. BPW	Calc. BYLP
A_1	2135/2138 (w)	2151 (78)	2095 (104)	2067 (82)
E	2052/2054 (vs)	2063 (1233)	2001 (1210)	1986 (1213)
A_1	2001/2007 (m)	2041 (680)	1999 (647)	1963 (659)
Calc. BVWN	Calc. VWN;COSMO			
	(CCl_4) $\varepsilon_R = 2.228$	(Cyclohexane) $\varepsilon_R = 2.015$	(Diethyl ether) $\varepsilon_R = 4.335$	($CHCl_3$) $\varepsilon_R = 4.806$
2058 (84)	2150 (142)	2152 (91)	2152 (111)	2152 (115)
1978 (1213)	2029 (2696)	2053 (1659)	2043 (2066)	2041 (2116)
1953 (647)	2007 (1496)	2027 (931)	2017 (1167)	2019 (1191)

[a] Wavenumbers in cm^{-1}.
[b] Relative intensities in parentheses; w = weak, m = medium, vs = very strong. calc. intensities in km mol^{-1}.
[c] IR active CO stretching modes.
[d] This work.

Table 5
IR data for $Mn_2(CO)_{10}$[a,b]

Band symmetry in D_{4d}[c]	Experimental (gas phase)[d]	Experimental (CCl_4)[e]	Calc. VWN	Calc. VWN, COSMO (CCl_4)
B_2	2053.3	2044 (s)	2078 (1262)	2076 (1358)
E_1	2026.1	2013 (vs)	2041 (2092)	2031 (2945)
B_2	1994.3	1983 (s)	2026 (713)	2012 (1335)

[a] Wavenumbers in cm^{-1}.
[b] Relative intensities in parentheses; s = strong, vs = very strong. calc. intensities in km mol^{-1}.
[c] IR active CO stretching modes.
[d] Ref. [32].
[e] This work.

Table 6
IR data for $MnCo(CO)_9$[a,b]

	Experimental (hexane)[c]/(CCl_4)[d]	Calc. VWN, C_s-symmetry COSMO (CCl_4)		Calc. VWN, C_{4v}-symmetry COSMO (CCl_4)	
A	2116.5 (0.004)/2117 (w)	2142 (42)	A_1	2148 (87)	ν_1
A	2056.2 (0.347)/2056 (vs)	2085 (1522)	A_1	2068 (1401)	ν_3
B	2045[e]	2060 (34)	B_1	2065 (10)	
E	2025.8 (1.0)/2024 (vs)	2042 (2371)	E	2052 (2135)	ν_5
E		2040 (2415)			ν_5
A	2004.0 (0.004)/2004 (sh,w)	2033 (192)	B_1	2019 (1)	ν_2
A	1996.0 (0.154)/1995 (m)	2021 (878)	A_1	2000 (648)	ν_4
E	1981.0 (0.111)/1977 (m)	2011 (87)	E	1995 (841)	ν_6
E		2005 (196)			ν_6

[a] Wavenumbers in cm^{-1}.
[b] Relative intensities in parentheses, sh = shoulder, m = medium, s = strong, vs = very strong. calc. intensities in km/mol.
[c] Ref. [18].
[d] This work.
[e] Ref. [10], calculated.

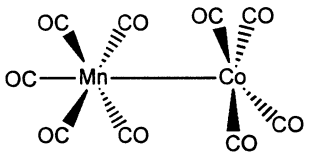

Fig. 2. Structure of $MnCo(CO)_9$ with hypothetical symmetry C_{4v}.

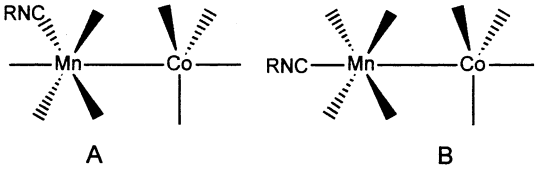

Fig. 3. Possible structures for $(CNR)(CO)_4MnCo(CO)_4$, (CO ligands omitted for clarity).

thus to test the ability of the calculations as a predictor of structure. The results are given in Table 6.

All calculated wavenumbers are too high (~ 20–30 cm^{-1}). The band patterns for both calculated spectra were very similar. Bor et al. based their assignment of the ν(CO) of $MnCo(CO)_9$ on a comparison of the IR spectrum of $MnCo(CO)_9$ to the IR spectra of $Mn_2(CO)_{10}$ (D_{4d}) and $HgCo_2(CO)_8$ (D_{3d}) [18]. Assignments of ν(CO) for the spectra calculated in this work were made based on the graphical display for each normal mode of vibration. The assignments of the ν(CO) for both calculated spectra were then compared to Bor's assignments.

The assignments for the C_s-structure calculations tally with Bor's assignments, while the assignments for C_{4v}-structure calculations differ from Bor's assignments. Frequency ν_2 for C_{4v} is a B mode localized on the Mn moiety, and not an A mode, corresponding to the symmetric stretch of the three equatorial COs on Co, as in Bor's assignment. Also, Sbrignadello computed from a complete set of force constants a B mode localized on the Mn moiety to be at 2045 cm^{-1} [10]. For C_s, the band calculated at 2060 cm^{-1} is a B mode localized on the Mn moiety, whereas for C_{4v} symmetry the B mode localized on the Mn moiety was calculated to be at 2019 cm^{-1}. The band calculated at 2065 cm^{-1} for C_{4v} is a B mode localized on the Co moiety. Keeping in mind that all calculated ν(CO) values are too high, the results for the Mn-localized B mode in C_s symmetry tally better with Sbrignadello's interpretation than the results obtained for C_{4v} symmetry.

Based on the assignments of the CO stretching frequencies, it is reasonable to assume that for the calculated spectrum in C_s symmetry, the bands at 2042 and 2040 cm^{-1}, as well as the bands at 2011 and 2005 cm^{-1}, could overlap in the experimental spectrum. The band calculated at 2060 (C_s) has an intensity of 34 and may therefore be invisible in the experimental spectrum. Hence, only six bands might be expected to be visible in the ν(CO) region.

For C_{4v}, the intensities of the bands at 2065 and 2019 cm^{-1} are 10 and 1, respectively, making them likely to be invisible in the IR spectrum. Consequently only five bands might be expected to be visible in the IR spectrum. Hence, the DMol calculations are consistent with the C_s symmetry for $MnCo(CO)_9$ suggested by Moosberry and Sheline [9].

The calculations suggest that accidental band overlap is the reason only six bands are observed in the IR spectrum of $MnCo(CO)_9$. Therefore the 'free rotational model' of Bor et al. is not the only possible explanation of the compound's IR spectrum.

The IR spectra of $MnCo(CO)_{9-n}(CNCH_3)_n$ ($n = 0$–2) were calculated using VWN as functionals, and employing the COSMO (CCl_4) model. The IR spectra of the complexes $MnCo(CO)_8(CNR)$ (R = 2,6-xylyl (**1**), t-butyl (**3**), n-butyl (**4**), 2,6-diisopropylphenyl (**8**), p-$MeOC_6H_4$ (**9**), p-ClC_6H_4 (**10**), p-MeC_6H_4 (**11**)) are listed in Table 7.

All complexes show one band (ν_1) due to coordinated CNR and 6 (**3** and **4**) or 7 (**1**, **8**, **9**, **10** and **11**) bands due to terminally coordinated CO. The reason why all alkyl isocyanide containing complexes show one ν(CO) band fewer in the IR spectrum than all aryl isocyanide containing complexes is probably overlap of ν_4 and ν_5. The spectra show no evidence of any bridging ligands. Group theory predicts 8 IR active ν(CO), regardless of

Table 7
IR data for $MnCo(CO)_8(CNR)$[a,b,c]

R = 2,6-xylyl (**1**)	R = t-butyl (**3**)	R = n-butyl (**4**)	R = 2,6-diisopropyl (**8**)	
2153 (m)	2175 (m)	2189 (m)	2154 (m)	ν_1
2080 (m)	2084 (m)	2086 (m)	2080 (m)	ν_2
2042 (s)	2040 (s)	2041 (s)	2042 (s)	ν_3
2015 (vs)			2016 (vs)	ν_4
2010 (vs)	2009 (vs)	2010 (vs)	2009 (vs)	ν_5
1974 (s)	1970 (s)	1972 (s)	1974 (s)	ν_6
1960 (m)	1956 (sh,m)	1952 (m)	1953 (m)	ν_7
1935 (vw)	1930 (vw)	1942 (vw)	1935 (vw)	ν_8

R = p-$MeOC_6H_4$ (**9**)	R = p-ClC_6H_4 (**10**)	R = p-MeC_6H_4 (**11**)	
2159 (m)	2153 (m)	2158 (m)	ν_1
2082 (m)	2080 (m)	2082 (m)	ν_2
2042 (s)	2043 (s)	2042 (s)	ν_3
2015 (vs)	2013 (vs)	2011 (vs)	ν_4
2012 (vs)	2000 (vs)	1996 (vs)	ν_5
1974 (s)	1976 (s)	1974 (s)	ν_6
1958 (m)	1962 (m)	1961 (m)	ν_7
1937 (vw)	1936 (vw)	1935 (vw)	ν_8

[a] Wavenumbers in cm^{-1}.
[b] Relative intensities in parentheses; vw = very weak, m = medium, s = strong, vs = very strong.
[c] In pentane.

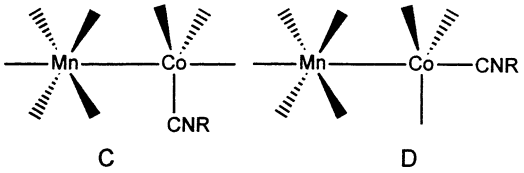

Fig. 4. Possible structures for $(CO)_5MnCo(CNR)(CO)_3$, (CO ligands omitted for clarity).

whether the CNR ligand is in equatorial (A, Fig. 3) or axial position (B, Fig. 3) on Mn.

Group theory also predicts eight bands due to ν(CO) in the IR spectrum for $(CO)_5MnCo(CO)_3(CNR)$, CNR in equatorial (C, Fig. 4) or axial position (D, Fig. 4).

However, the band pattern should be different for each structure, and ideally only one should resemble the pattern of the experimental spectrum. Therefore we calculated the IR spectra for structures A, B, C and D to determine whether calculations lead to a unique assignment of structure. IR spectra for A, B, C and D were calculated with $R = CH_3$ to minimize computational effort. The calculated spectra were compared with the measured spectrum of **9**. An aryl isocyanide complex was chosen as comparison because of the good band resolution. The absolute values of the calculated ν(CO), given in Table 8, are all too high (~ 30 cm^{-1}).

In order to compare the calculated spectra with the experimental spectra, the average deviations of all computed frequencies from the experimental spectrum of **9** were calculated. ν(CN) was not included in the calculation of the average deviation because its energy greatly depends on the nature of R. Since CH_3 was chosen as R for the calculations, ν(CN) is expected to be calculated at higher wavenumbers, than for any other R group [4].

The average deviations, given in Table 8, show that structures A and B have similar deviations from the experimental values, whereas structures C and D show similar but significantly higher deviations. Therefore, the calculations indicate that structures C and D are unlikely structures for $MnCo(CO)_8(CNR)$.

For structure A, the band calculated at 2016 cm^{-1} (ν_6), which corresponds to an A_{1g} mode in point group D_{3d}, is probably not resolved in the experimental spectrum. Its intensity is small compared to the intensity of the 2024 cm^{-1} band, so that it may be hidden in the tail of the 2024 cm^{-1} band. Hence seven bands are expected to be observed in the ν(CO) region. For structure B ν_6 was calculated at 2041 cm^{-1}. Again, keeping in mind that all calculated wavenumbers are too high by 20–30 cm^{-1}, one would expect to see this band at $\sim$2010–2020 cm^{-1} in the experimental spec-

Table 8
Comparison of experimental and calculated IR data for $MnCo(CO)_8(CNR)$[a,b]

R = *p*-$MeOC_6H_4$ (**9**) experimental (pentane)	R = CH_3, calc. VWN COSMO (CCl_4) equatorial, A	R = CH_3, calc. VWN COSMO (CCl_4) axial, B	
2159 (m)	2258 (529)	2246 (1161)	ν_1
2082 (m)	2110 (332)	2108 (382)	ν_2
2042 (s)	2068 (1650)	2065 (840)	ν_3
2015 (vs)	2036 (1179)	2019 (2728)	ν_4
2012 (vs)	2024 (2524)	2017 (2311)	ν_5
	2016 (92)	2041 (78)	ν_6
1974 (s)	2000 (1246)	2012 (553)	ν_7
1958 (m)	1993 (267)	1988 (23)	ν_8
1937 (vw)	1990 (221)	1984 (69)	ν_9
Average deviation	23	22	
	R = CH_3, calc. VWN COSMO (CCl_4) equatorial, C	R = CH_3, calc. VWN COSMO (CCl_4) axial, D	
	2222 (649)	2264 (955)	ν_1
	2119 (598)	2122 (520)	ν_2
	2061 (1666)	2032 (850)	ν_3
	2048 (521)	2027 (2246)	ν_4
	2029 (1149)	2025 (2225)	ν_5
	2019 (1796)	2045 (43)	ν_6
	2012 (620)	2011 (689)	ν_7
	2010 (974)	1989 (214)	ν_8
	1989 (181)	1982 (358)	ν_9
Average deviation	31	36	

[a] Wavenumbers in cm^{-1}.

[b] Relative intensities in parentheses; vw = very weak, m = medium, s = strong, vs = very strong. Calculated intensities in km mol^{-1}.

Table 9
IR data for $MnCo(CO)_7(CNR)_2$[a,b,c]

R = 2,6-xylyl (**2**)	R = *p*-$MeOC_6H_4$ (**6**)	R = t-butyl (**7**)	R = n-butyl (**12**)	R = 2,6-diisopropyl (**13**)	
2152 (w)	2159 (w)	2172 (w)	2185 (w)	2153 (w)	ν_1
2119 (m)	2129 (m)	2148 (m)	2162 (m)	2119 (m)	ν_2
2106 (m)	2115 (m)	2133 (m)	2148 (m)	2108 (m)	ν_3
2050 (s)	2050 (s)	2050 (s)	2053 (s)	2049 (s)	ν_4
2027 (m)	2028 (m)	2023 (m)	2025 (m)	2028 (m)	ν_5
2018 (vs)	2018 (vs)	2015 (vs)	2017 (vs)	2018 (vs)	ν_6
1994 (vs)	1994 (vs)	1988 (vs)	1989 (vs)	1993 (vs)	ν_7
1955 (s)	1954 (s)		1957 (s)	1954 (s)	ν_8
		1947 (s)	1949 (s)		ν_9

[a] In pentane.
[b] Wavenumbers in cm^{-1}.
[c] Relative intensities in parentheses; vw = very weak, w = weak, m = medium, s = strong, vs = very strong.

trum. This band would very likely be obscured in the experimental spectrum by ν_4 and ν_5. Additionally the band calculated at 1988 cm^{-1} (ν_8) has a very low intensity, making it likely to be invisible in the IR spectrum. Therefore, only 6 bands would be visible in the ν(CO) region.

Overall, the calculated spectrum for structure A tallies best with the experimental spectrum of **9**. The DMol calculations lead to a unique assignment of the structure for **9**; this agrees with the structure of **1** determined by X-ray diffraction. For $MnCo(CO)_8(CNR)$, ν(CN) is shifted to higher wavenumbers compared to $Mn_2(CO)_9(CNR)$ (R = t-butyl, 2,6-xylyl). The more positive the oxidation state of a metal, the higher ν(CN) is [34]. Since the $Co(CO)_4$ moiety withdraws electron density from the Mn moiety, ν(CN) is expected to be at higher wavenumbers. Also, the highest totally symmetric ν(CO) (ν_2), symmetric on Mn and Co, is shifted to lower wavenumbers, compared to $MnCo(CO)_9$. This is due to the fact that CNR is a better overall electron-donor than CO. More electron density around the Mn center strengthens the Mn–C bond; hence the CO bond is weakened. As a result ν(CO) is lowered.

The IR spectra of $MnCo(CO)_7(CNR)_2$ (R = 2,6-xylyl (**2**), *p*-$MeOC_6H_4$ (**6**), t-butyl (**7**), n-butyl (**12**), 2,6-diisopropylphenyl (**13**)) are listed in Table 9.

Surprisingly, the spectra exhibit two medium and one weak absorptions due to the two terminal CNR groups (> 2100 cm^{-1}). A possible explanation is that in solution different isomers exist. The two CNR ligands in the second isomer could be in equatorial-*trans* position to each other or in axial-equatorial position. The first structure would make two *trans* CO ligands compete for electrons, which is unlikely. The band position of the highest ν(CN) in the IR spectra of $MnCo(CO)_7(CNR)_2$ is very close to ν(CN) of the corresponding $MnCo(CO)_8(CNR)$; however repeated recystallization of $MnCo(CO)_7(CNR)_2$ did not change the relative band intensities. Therefore it seems unlikely that all of the samples of $MnCo(CO)_7(CNR)_2$ are contaminated with $MnCo(CO)_8(CNR)$. The synthesis of **1** has shown that the Mn–CNR bond is rather labile; still it seems unlikely that an isomer with the CNR group in axial position exists for $MnCo(CO)_7(CNR)_2$, but not for $MnCo(CO)_8(CNR)$. Alternatively, one of the high-energy bands might be a combination band.

The complexes show six (**12**) or five bands (**2**, **6**, **7**, and **13**) due to terminal CO stretching in the IR spectrum, instead of the seven bands group theory predicts. The IR spectrum of $MnCo(CO)_7(CNCH_3)_2$ was calculated for two possible structural isomers, *eq,eq-cis*-$(CNCH_3)_2(CO)_3MnCo(CO)_4$ (E, Fig. 5) and *ax,eq*-$(CNCH_3)_2(CO)_3MnCo(CO)_4$ (F, Fig. 5).

The results of the calculations are given in Table 10.

The results were compared to the IR spectrum of **12**, because the IR spectrum of this complex showed the best resolution of ν(CO). In all other IR spectra of $MnCo(CO)_7(CNR)_2$ complexes ν_8 and ν_9 (Table 9) probably overlap. For reasons mentioned above, ν(CN) were not included in the calculation of the average deviation of the calculated wavenumbers from the experimentally obtained wavenumbers. All calculated band positions are too high, except for ν_6. The average deviation for structures E and F is 22 and 17 cm^{-1}, respectively. So, no choice between the structures is possible on this basis. Both calculated spectra exhibit an additional band (ν_{10}), not seen in the experimental spectrum. ν_{10} has a weak intensity for E (145), and a very strong intensity for F (1368). For structure E, ν_{10} might be obscured in the experimental spectra, since it

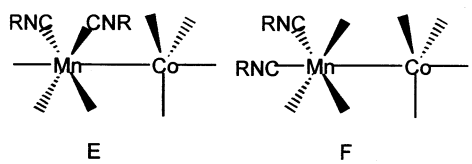

Fig. 5. Possible structures for $(CNR)_2(CO)_3MnCo(CO)_4$, (CO ligands omitted for clarity).

Table 10
Comparison of experimental and calculated IR data for $Mn-Co(CO)_7(CNR)_2$[a,b]

	Experimental R = n-butyl (**12**)	R = CH_3, calc. VWN, COSMO (CCl_4); E	R = CH_3, calc. VWN, COSMO (CCl_4); F
ν_1	2185 (w)	2251 (511)	2260 (1047)
ν_2	2162 (m)	2222 (674)	2221 (930)
ν_3	2148 (m)		
ν_4	2053 (s)	2084 (683)	2082 (1081)
ν_5	2025 (m)	2051 (1676)	2044 (899)
ν_{10}		2023 (145)	2018 (1368)
ν_6	2017 (vs)	2009 (1216)	2000 (319)
ν_7	1989 (vs)	1997 (492)	1995 (1760)
ν_8	1957 (s)	1992 (325)	1975 (1157)
ν_9	1949 (s)	1975 (390)	1962 (239)
Average deviation		22	17

[a] Wavenumbers in cm^{-1}.
[b] Relative intensities in parentheses; w = weak, m = medium, s = strong, vs = very strong. calc.intensities in km mol^{-1}.

lies on the tail of a very strong band. For structure F the calculated intensity of ν_{10} makes it impossible for ν_{10} to be obscured in the experimental spectra. Hence six ν(CO) bands are expected for structure E, whereas seven ν(CO) bands are expected for structure F.

A unique assignment of the structure based on the DMol calculations, which was possible in the case of $MnCo(CO)_8(CNR)$, cannot be made for $Mn-Co(CO)_7(CNR)_2$. As for the number of ν(CO) bands, the spectrum calculated for E tallies better with the spectrum of **12**; but the absolute values of wavenumbers of ν(CO) for F tally a little better with the experimental values.

Table 11
Bond lengths (Å) for **1**[a]

Mn(1)–C(5)	1.775(5)	Mn(1)–C(6)	1.840(4)
Mn(1)–C(8)	1.845(5)	Mn(1)–C(7)	1.854(5)
Mn(1)–C(9)	1.936(4)	Mn(1)–Co(1)	2.870(1)
Co(1)–C(3)	1.778(7)	Co(1)–C(1)	1.780(5)
Co(1)–C(2)	1.782(6)	Co(1)–C(4)	1.797(5)
O(1)–C(1)	1.131(5)	O(2)–C(2)	1.142(6)
O(3)–C(3)	1.140(6)	O(4)–C(4)	1.140(5)
O(5)–C(5)	1.152(5)	O(6)–C(6)	1.138(4)
O(7)–C(7)	1.142(5)	O(8)–C(8)	1.149(5)
N(1)–C(9)	1.157(4)	N(1)–C(10)	1.404(5)
C(10)–C(11)	1.385(5)	C(10)–C(15)	1.387(5)
C(11)–C(12)	1.390(5)	C(11)–C(17)	1.503(6)
C(12)–C(13)	1.363(6)	C(13)–C(14)	1.367(6)
C(14)–C(15)	1.392(6)	C(15)–C(16)	1.513(6)

[a] Estimated standard deviations in the least significant figure are given in parentheses.

Table 12
Bond angles (°) for **1**[a]

C(5)–Mn(1)–C(6)	91.6(2)	C(5)–Mn(1)–C(8)	92.4(2)
C(6)–Mn(1)–C(8)	91.6(2)	C(5)–Mn(1)–C(7)	93.6(2)
C(6)–Mn(1)–C(7)	92.0(2)	C(8)–Mn(1)–C(7)	172.9(2)
C(5)–Mn(1)–C(9)	88.8(2)	C(6)–Mn(1)–C(9)	178.2(2)
C(8)–Mn(1)–C(9)	86.7(2)	C(7)–Mn(1)–C(9)	89.8(2)
C(5)–Mn(1)–Co(1)	172.52(13)	C(6)–Mn(1)–Co(1)	82.17(13)
C(8)–Mn(1)–Co(1)	91.89(14)	C(7)–Mn(1)–Co(1)	82.56(13)
C(9)–Mn(1)–Co(1)	97.60(12)	C(3)–Co(1)–C(1)	95.1(2)
C(3)–Co(1)–C(2)	125.2(3)	C(1)–Co(1)–C(2)	96.9(2)
C(3)–Co(1)–C(4)	115.4(2)	C(1)–Co(1)–C(4)	97.4(2)
C(2)–Co(1)–C(4)	115.6(2)	C(3)–Co(1)–Mn(1)	82.7(2)
C(1)–Co(1)–Mn(1)	176.0(2)	C(2)–Co(1)–Mn(1)	81.7(2)
C(4)–Co(1)–Mn(1)	86.59(13)	C(9)–N(1)–C(10)	176.1(4)
O(1)–C(1)–Co(1)	178.9(5)	O(2)–C(2)–Co(1)	174.1(4)
O(3)–C(3)–Co(1)	174.0(5)	O(4)–C(4)–Co(1)	177.9(4)
O(5)–C(5)–Mn(1)	178.9(5)	O(6)–C(6)–Mn(1)	177.0(4)
O(7)–C(7)–Mn(1)	178.7(4)	O(8)–C(8)–Mn(1)	176.4(4)
O(9)–C(9)–Mn(1)	172.5(4)	C(11)–C(10)–C(15)	123.7(4)
C(11)–C(10)–N(1)	118.2(4)	C(15)–C(10)–N(1)	118.0(4)
C(10)–C(11)–C(12)	116.7(4)	C(10)–C(11)–C(17)	121.7(4)
C(12)–C(11)–C(17)	121.6(4)	C(13)–C(12)–C(11)	121.2(5)
C(12)–C(13)–C(14)	120.8(4)	C(13)–C(14)–C(15)	120.9(4)
C(10)–C(15)–C(14)	116.7(4)	C(10)–C(15)–C(16)	121.4(4)
C(14)–C(15)–C(16)	121.9(4)		

[a] Estimated standard deviations in the least significant figure are given in parentheses.

3.4. Structures of $MnCo(CO)_8$(2,6-xylyl)NC (**1**) and $MnCo(CO)_7$((2,6-xylyl)NC)$_2$ (**2**)

Crystals of **1** (orange–red) and **2** (dark red), suitable for an X-ray crystallographic study, were obtained from pentane at −25°C. Bond angles and bond lengths for **1** and **2** are given in Tables 11–14.

Table 13
Bond lengths (Å) for **2**[a]

Co(1)–C(6)	1.769(5)	Co(1)–C(5)	1.770(4)
Co(1)–C(4)	1.774(4)	Co(1)–C(7)	1.800(5)
Co(1)–Mn(1)	2.9035(7)	Mn(1)–C(1)	1.785(4)
Mn(1)–C(2)	1.838(4)	Mn(1)–C(3)	1.841(4)
Mn(1)–C(8)	1.924(4)	Mn(1)–C(17)	1.941(3)
O(1)–C(1)	1.148(4)	O(2)–C(2)	1.139(4)
O(3)–C(5)	1.138(5)	O(4)–C(4)	1.151(4)
O(5)–C(5)	1.143(4)	O(6)–C(6)	1.141(5)
O(7)–C(7)	1.138(5)	N(1)–C(8)	1.160(4)
N(1)–C(9)	1.413(5)	N(2)–C(17)	1.153(4)
N(2)–C(18)	1.402(4)	C(9)–C(10)	1.347(6)
C(9)–C(14)	1.425(6)	C(10)–C(11)	1.449(7)
C(10)–C(16)	1.485(7)	C(11)–C(12)	1.449(7)
C(12)–C(13)	1.352(8)	C(13)–C(14)	1.379(6)
C(14)–C(15)	1.485(7)	C(18)–C(19)	1.394(5)
C(18)–C(23)	1.397(5)	C(19)–C(20)	1.400(5)
C(19)–C(25)	1.499(5)	C(20)–C(21)	1.368(6)
C(21)–C(22)	1.362(6)	C(22)–C(23)	1.379(5)
C(23)–C(24)	1.499(5)		

[a] Estimated standard deviations in the least significant figure are given in parentheses.

Table 14
Bond angles (°) for **2**[a]

C(6)–Co(1)–C(5)	94.7(2)	C(6)–Co(1)–C(4)	96.6(2)
C(5)–Co(1)–C(4)	126.5(2)	C(6)–Co(1)–C(7)	99.8(2)
C(5)–Co(1)–C(7)	114.4(2)	C(4)–Co(1)–C(7)	114.6(2)
C(6)–Co(1)–Mn(1)	169.5(2)	C(5)–Co(1)–Mn(1)	78.68(12)
C(4)–Co(1)–Mn(1)	80.91(12)	C(7)–Co(1)–Mn(1)	90.46(13)
C(1)–Mn(1)–C(2)	92.8(2)	C(1)–Mn(1)–C(3)	90.5(2)
C(2)–Mn(1)–C(3)	94.5(2)	C(1)–Mn(1)–C(8)	90.1(2)
C(2)–Mn(1)–C(8)	89.9(2)	C(3)–Mn(1)–C(8)	175.56(14)
C(1)–Mn(1)–C(17)	91.3(2)	C(2)–Mn(1)–C(17)	173.0(2)
C(3)–Mn(1)–C(17)	91.14(14)	C(8)–Mn(1)–C(17)	84.44(13)
C(1)–Mn(1)–Co(1)	170.03(12)	C(2)–Mn(1)–Co(1)	80.42(12)
C(3)–Mn(1)–Co(1)	82.84(12)	C(8)–Mn(1)–Co(1)	97.13(10)
C(17)–Mn(1)–Co(1)	96.17(9)	C(8)–N(1)–C(9)	177.8(3)
C(17)–N(2)–C(18)	176.7(3)	O(1)–C(1)–Mn(1)	178.9(4)
O(2)–C(2)–Mn(1)	177.2(3)	O(3)–C(3)–Mn(1)	176.7(3)
O(4)–C(4)–Co(1)	173.5(3)	O(5)–C(5)–Co(1)	173.0(3)
O(6)–C(6)–Co(1)	179.4(5)	O(7)–C(7)–Co(1)	177.5(4)
N(1)–C(8)–Mn(1)	173.9(3)	C(10)–C(9)–N(1)	118.5(4)
C(10)–C(9)–C(14)	124.3(4)	N(1)–C(9)–C(14)	117.2(4)
C(9)–C(10)–C(11)	118.5(5)	C(9)–C(10)–C(16)	121.6(4)
C(11)–C(10)–C(16)	119.9(5)	C(12)–C(11)–C(10)	115.1(6)
C(13)–C(12)–C(11)	126.6(6)	C(12)–C(13)–C(14)	119.3(6)
C(13)–C(14)–C(9)	116.1(5)	C(13)–C(14)–C(15)	122.2(5)
C(9)–C(14)–C(15)	121.7(4)	N(2)–C(17)–Mn(1)	174.6(3)
C(19)–C(18)–C(23)	123.9(3)	C(19)–C(18)–N(2)	118.9(3)
C(23)–C(18)–N(2)	117.2(3)	C(18)–C(19)–C(20)	115.5(4)
C(18)–C(19)–C(25)	121.8(3)	C(20)–C(19)–C(25)	122.7(4)
C(21)–C(20)–C(19)	121.6(4)	C(22)–C(21)–C(20)	120.7(4)
C(21)–C(22)–C(23)	121.3(4)	C(22)–C(23)–C(18)	116.9(3)
C(22)–C(23)–C(24)	121.3(4)	C(18)–C(23)–C(24)	121.8(3)

[a] Estimated standard deviations in the least significant figure are given in parentheses.

ORTEP drawings for **1** and **2** are presented in Figs. 6 and 7, respectively. For both complexes the coordination geometry around the Co center is trigonal–bipyramidal, and octahedral around the Mn center. Both complexes contain a single metal–metal bond and no bridging ligands. The overall symmetry is C_1 for **1** and C_s for **2**. To the best of our knowledge, these are the first crystal structures reported for an unbridged Mn–Co carbonyl complex. The isocyanide ligand on Mn in **1** is in an equatorial position. The two isocyanides on Mn in complex **2** are in *cis*-equatorial position to each other. This is similar to those in 1,1-$Mn_2(CO)_8$((t-butyl)NC)$_2$ [35] and $Re_2(CO)_{10-n}(CNR)_n$ ($n = 1$, R = t-butyl; $n = 2$, R = 2,6-xylyl) [5b]. The probable reason for this is that CO is a very strong π-acceptor. Therefore two CO ligands *trans* to each other compete for electron density, weakening the metal–C bond. CNR is a considerably weaker π-acceptor; hence it is less electron-withdrawing than a CO from the opposite CO group, stabilizing the metal–carbonyl bond.

The Mn–Co bond lengths of 2.870(1) Å in **1** and 2.9035(7) Å in **2** are similar to the Mn–Mn bond length in $Mn_2(CO)_{10}$ (2.895(1) Å) [36] and 1,1-$Mn_2(CO)_8$((t-butyl)NC)$_2$ (2.924(1) Å) [35]. In contrast, the Co–Co bond length in $Co_2(CO)_8$ (2.528(1) Å) [37] and in Co_2((t-butyl)NC)$_8$ (2.4557 Å) [38] is much shorter. This is partly due to the two bridging ligands, but even for the 'high temperature' isomer of $Co_2(CO)_8$, $(CO)_3CoCo(CO)_3$ with six terminal carbonyls, the Co–Co bond length was calculated to be 2.634 Å [39]. Although the bond length of $MnCo(CO)_9$ is unknown, it can be assumed that the substitution of two CO by two CNR ligands does not increase the bond length dramatically. For example, the difference in the Re–Re bond length between $Re_2(CO)_{10}$ and $Re_2(CO)_8$((2,6-xy-

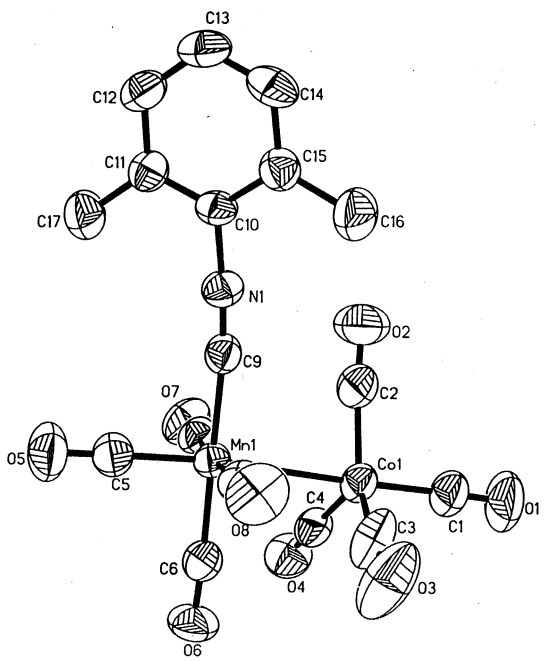

Fig. 6. ORTEP drawing of complex **1**.

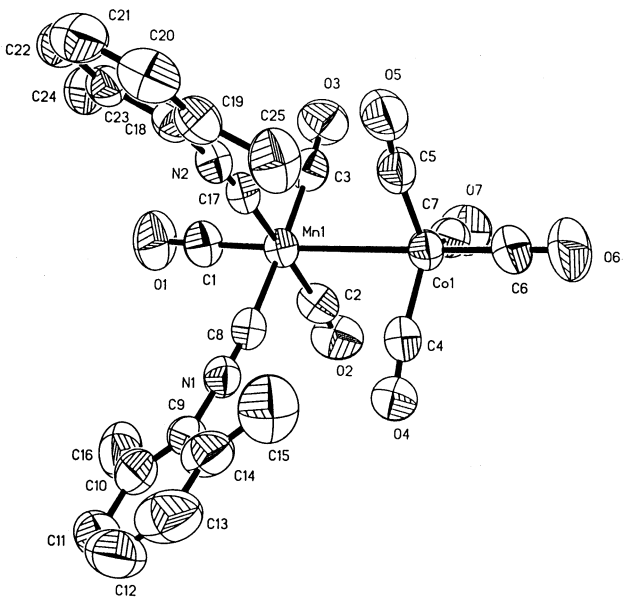

Fig. 7. ORTEP drawing of complex **2**.

lyl)NC)$_2$ is only 0.007 Å [5b]. Mn–Co bond lengths reported in the literature are only for molecules containing bridging ligands. For example [CoMn(CO)$_6$-(Ph$_2$C$_4$Me$_2$)] has a Mn–Co bond length of 2.5488(8) Å [40], [σ^2-N, σ^2-N′, η^2-C=N-[glyoxalbis(t-butylimine)]]hexacarbonyl cobalt manganese has a Mn–Co bond length of 2.639(3) Å [41], and MnCo(CO)$_3$(μ^2-CO)$_2$(μ^2-Ph$_2$PCH$_2$PPh$_2$)$_2$ has a Mn–Co bond length of 2.726 Å [42].

Surprisingly the CNR group in **1** and both CNR groups in **2** are in eclipsed position relative to CO groups on Co. This indicates very little steric interaction between CNR on Mn and CO on Co.

The Mn–CO distances in **1** [Mn–CO$_{ax}$: 1.775(5) Å; Mn–CO$_{eq}$: 1.854(5) Å, 1.845(4) Å, 1.840(4) Å] and **2** [Mn–CO$_{ax}$: 1.7854(4) Å; Mn–CO$_{eq}$: 1.838(4) Å, 1.841(4) Å] are longer, than those observed for 1,1-Mn$_2$(CO)$_8$((t-butyl)NC)$_2$ [Mn–CO$_{ax}$: 1.748(5) Å; Mn–CO$_{eq}$: 1.824(5) Å] [35]. The Mn–CNR distances in **1** (1.936(4) Å) and **2** (1.924(4) Å, 1.941(4) Å) are shorter, than in 1,1-Mn$_2$(CO)$_8$((t-butyl)NC)$_2$ (1.944(4) Å) [35]. The reason for this is probably the enhanced π-backbonding ability of aryl isocyanides compared to alkyl isocyanides [43].

The Co–CO$_{eq}$ distances in **1** (1.778(7), 1.782(6) and 1.797(5) Å) and **2** (1.774(4), 1.770(4) and 1.800(5) Å) are shorter than those in HCo(CO)$_4$ (1.818(3) Å) [44] and in Co$_2$(CO)$_8$ (1.827(2) Å) [37], supporting the statement that the electron density around the Co is increased compared to Co$_2$(CO)$_8$. Increased electron density increases the Co→CO π-backbonding; hence the Co–CO distances decrease. However the Co–CO$_{ax}$ bond in **1** (1.780(5) Å) and **2** (1.769(5) Å) are longer than in HCo(CO)$_4$ (1.764(10) Å) [44]. This might be attributed to the fact that the structure of HCo(CO)$_4$ was determined by electron diffraction, and not by X-ray diffraction.

Less Mn→CO π-backbonding means a shorter C–O bond length, because less electron density is pushed into the π* orbital of CO. Therefore the MnC–O bond lengths in **1** and **2** might be expected to be shorter compared to Mn$_2$(CO)$_{10}$. However, the observed average MnC–O bond lengths for **2** and Mn$_2$(CO)$_{10}$ are the same (1.142 Å) [36], whereas the average MnC–O bond lengths in **1** (1.145(5) Å) are only slightly longer than in Mn$_2$(CO)$_{10}$. The differences in the MnC–O bond lengths are within the experimental error and no definite conclusions can be made.

Most of the M–C–O angles in **1** and **2** are close to 180°. The two Co–C–O angles opposite the two CNR ligands are smaller (173.0(3) and 173.5(3)°) than the third equatorial Co–C–O angle (177.5(4)°). This could indicate a slight steric interaction between the COs and the eclipsing CNR ligands; however, the energy involved is apparently not large enough to lead to a staggered geometry. Although in Co$_2$(CO)$_8$ the Co–C$_{terminal}$–O angles are in fact closer to 180° (174.9(1)–178.9(1)°) [37], supporting this reasoning, the Co–C$_{eq}$–O angles in HCo(CO)$_4$ are even smaller (172.6(1.2)°) than in **2** [44]. However, the CO$_{eq}$ ligands in HCo(CO)$_4$ are bent towards the fifth ligand H, and not away as in **2**. In compound **1** the Co–C$_{eq}$–O angle opposite the CNR ligand on Mn is closer to 180° (177.9(4)°) than the other two Co–C$_{eq}$–O angles (174.1(4) and 174.0(5)°), although the Mn–Co bond length in **1** is shorter than in **2**. Therefore steric interactions seem unlikely to be the cause for the Co–C$_{eq}$–O angles in **1** and **2** to be unequal. It remains unclear why in complexes **1** and **2** two of the three equatorial carbonyls on Co are more bent.

4. Conclusions

The chemistry of MnCo(CO)$_9$ towards CNR is closely related to that of Mn$_2$(CO)$_{10}$. The substitution site on MnCo(CO)$_9$ is the Mn center. Similar to Mn$_2$(CO)$_{10}$, the number of coordinated CNR per Mn never exceeds two. The CNR ligands are always in equatorial position, terminally coordinated and, if more than one, are in *cis* position to each other for both Mn$_2$(CO)$_{10}$ and MnCo(CO)$_9$ derivatives.

The calculation of IR spectra employing DFT methods proved to be a useful tool in the assignment of CO stretching bands for MnCo(CO)$_9$. A unique assignment of structure for the complexes MnCo(CO)$_{9-n}$(CNR)$_n$, based on the compound's calculated IR spectra, was possible only for $n=1$. It appears that the higher the degree of substitution of CO by CNR is, the less definitive the results of the DMol calculations are. We are currently investigating the reactivity of the complexes MnCo(CO)$_{9-n}$(CNR)$_n$ towards alkynes and alkenes, under Pauson–Khand reaction conditions.

5. Supplementary material

Crystallographic data (excluding structure factors) for the structures reported in this paper have been deposited with the Cambridge Crystallographic Data Centre as supplementary publication no. CCDC-103060 (Compound **1**) and CCDC-103061 (Compound **2**). Copies of the data can be obtained free of charge on application to CCDC, 12 Union Road, Cambridge CB2 1EZ, UK (fax: +44-1223-336 033; E-mail: deposit@ccdc.cam.ac.uk). Structure factors are available upon request from the authors.

Acknowledgements

Crystallographic data were collected through the Ohio Crystallographic Consortium, funded by the Ohio Board of Regents 1995 Investment Fund (CAP-075), located at the University of Toledo, Instrumentation Center in A&S, Toledo, OH 43606. We thank Professor Thomas L. Beck for useful conversations. JAKB sincerely thanks Dr Ewa Skrzypczak-Jankun (University of Toledo) for assistance in using the CCD diffractometer system. KB gratefully acknowledges a Millenium Petrochemicals graduate fellowship.

References

[1] (a) W.A. Herrmann, B. Cornils, Angew. Chem., Int. Ed. Engl. 36 (1997) 1048. (b) W.R. Moser, D.W. Slocum (Eds.), Homogeneous Transition Metal Catalyzed Reactions, American Chemical Society Advances in Chemistry Series, vol. 230, Washington, DC, 1992.
[2] S.A. Lanemann, G.G. Stanley, in: W.R. Moser, D.W. Slocum (Eds.), Homogeneous Transition Metal Catalyzed Reactions, American Chemical Society Advances in Chemistry Series, vol. 230, Washington, DC, 1992, p. 349.
[3] F.A. Cotton, G. Wilkinson, Advanced Inorganic Chemistry, 5th Edn., Wiley, New York, 1988, p. 255 and references therein.
[4] (a) M.O. Albers, N.J. Coville, S. Afr. J. Chem. 35 (1982) 139. (b) G.W. Harris, N.J. Coville, J. Cryst. Spectros. Res. 19 (1989) 451.
[5] (a) G.W. Harris, N.J. Coville, Organometallics 4 (1985) 908. (b) G.W. Harris, J.C.A. Boeyens, N.J. Coville, Organometallics 4 (1985) 914. (c) G.W. Harris, N.J. Coville, J. Cryst. Spectros. Res. 19 (1989) 451.
[6] Y Yamamoto, H. Yamazaki, Inorg. Chem. 17 (1978) 3111.
[7] G.K. Barker, A.M.R. Galas, M. Green, J.A.K. Howard, F.G.A. Stone, T.W. Turney, A.J. Welch, P. Woodward, J. Chem. Soc., Chem. Commun. (1977) 256.
[8] (a) K.K. Joshi, P.L. Pauson, Z. Naturforsch. 76 (1962) 565. (b) T. Kruck, M. Hofler, Chem. Ber. 97 (1964) 2289.
[9] E.S. Moosberry, R.K. Sheline, J Chem. Phys. 56 (1972) 1852.
[10] G. Sbrignadello, Inorg. Chim. Acta 48 (1981) 237.
[11] E.E. Ernstbrunner, M. Kilner, J. Chem. Soc., Dalton Trans. (1976) 417.
[12] R. Obrecht, R.H. Herrmann, I. Ugi, Synthesis (1985) 400.
[13] R. Appel, R. Kleinstück, K.-D. Ziehn, Angew. Chem., Int. Ed. Engl. 10 (1971) 132.
[14] W. Hieber, O. Vohler, G. Braun, Z. Naturforsch., Teil B 13 (1958) 192.
[15] P.A. Leach, S.J. Geib, J.A. Corella II, G.F. Warnock, N.J. Cooper, J. Am. Chem. Soc. 116 (1994) 8566.
[16] R.B. King, Organometallic Synthesis, vol. 1, Academic Press, New York, 1965, p. 174.
[17] N.J. Coville, P. Johnston, A.E. Leins, A.J. Markwell, J. Organomet. Chem. 378 (1989) 401.
[18] G. Sbrignadello, G. Bor, L. Maresca, J. Organomet. Chem. 46 (1972) 345.
[19] (a) DMol and Insight II are commercially available from Molecular Simulations, 9685 Scranton Road, San Diego, CA 92121-3752. (b) DMol user manual, p. 85.
[20] S.H. Vosko, L. Wilk, M. Nusair, Can. J. Phys. 58 (1980) 1200.
[21] A.D. Becke, Phys. Rev. A38 (1988) 3098.
[22] J.P. Perdew, Y. Wang, Phys. Rev. B45 (1992) 13244.
[23] C. Lee, W. Yang, R.G. Parr, Phys. Rev B37 (1988) 785.
[24] (a) A. Klamt, G. Schüürmann, J. Chem. Soc., Perkin Trans. II (1993) 799. (b) J. Andzelm, C. Kölmel, A. Klamt, J. Chem. Phys. 21 (1995) 9312. (c) A. Klamt, V. Jonas, T. Bürger, J.C.W. Lohrenz, J. Phys. Chem. A 102 (1998) 5074.
[25] The SMART v4.05 and SAINT v4.05, Siemens Analytical X-ray Instruments, Inc., Madison, WI.
[26] SADABS, G.M. Sheldrick, University of Göttingen, Germany.
[27] SHELXTL v5.03, G.M. Sheldrick, University of Göttingen, Germany, and Siemens Analytical X-ray Instruments, Inc., Madison, WI.
[28] J.K. Shen, Y.-C. Gao, Q. Zhen, F. Basolo, Organometallics 8 (1989) 2144, and leading references therein.
[29] H.K. Van Dijk, J. van der Haar, D.J. Stufkens, A. Oskan, Inorg. Chem. 28 (1989) 75.
[30] R.B. King, M.S. Saran, Inorg. Chem. 11 (1972) 2115.
[31] (a) L. Fan, T. Ziegler, J. Phys. Chem. 96 (1992) 6937. (b) W. Thiel, M. Bühl, Inorg. Chem. 36 (1997) 2922. (c) A. Bérces, J. Phys. Chem. 100 (1996) 16538. (d) V. Jonas, W. Thiel, Organometallics 17 (1998) 353.
[32] N.J. Gould, D.J. Parker, Spectrochim. Acta, Part A 31 (1975) 1785.
[33] G. Bor, J. Organomet. Chem. 65 (1974) 81.
[34] P.M. Treichel, in: F.G.A. Stone, R. West (Eds.), Advances in Organometallic Chemistry, vol. 11, Academic Press, New York, 1973, p. 24.
[35] D.J. Robinson, G.W. Harris, J.C.A. Boeyns, N.J. Coville, J. Chem. Soc., Chem. Commun. (1984) 1307.
[36] M Martin, B. Rees, A. Mitschler, Acta Crystallogr., Sect. B 38 (1982) 6.
[37] P.C. Leung, C. Coppens, Acta Crystallogr., Sect. B 39 (1983) 535.
[38] W.E. Carrol, M. Green, A.M.R. Galas, M. Murray, W.T. Terence, A.J. Welch, P. Woodward, J. Chem. Soc., Dalton Trans. (1980) 80.
[39] E. Folga, T. Ziegler, J. Am. Chem. Soc. 115 (1993) 5169.
[40] F.W.B. Einstein, P. Manning, L.K. Peterson, K.G. Tyes, Inorg. Chim. Acta 111 (1986) L49.
[41] L.H. Staal, G. van Koten, K. Vrieze, J.A. Cras, W.P. Bosman, Inorg. Chem. 20 (1981) 555.
[42] D.J. Elliot, D.G. Holah, A.N. Hughes, J.J. Vittal, P.J. Puddephatt, Organometallics 12 (1993) 1225.
[43] P.M. Treichel, in: F.G.A. Stone, R. West (Eds.), Advances in Organometallic Chemistry, vol. 11, Academic Press, New York, 1973, p. 26.
[44] E.A. McNeill, F.R. Scholer, J. Am. Chem. Soc. 99 (1977) 6243.